Design, Fabrication and Analysis of Interferometers in SOI Photonics

Abishek Nair

Abstract

This report describes the design of Mach-Zehnder Interferometers (MZIs) for silicon-on-insulator (SOI) fabrication, using waveguides in the strip configuration. Simulated results and analytical evaluations are presented to support the design decisions. Experimental data is compared with simulations to validate the design and fabrication process. An error of less than 1% was achieved in the estimation of the group index for the TE mode at 1550 nm.

Introduction

With the ever-increasing demand for higher bandwidth, the need for innovative solutions to overcome communication challenges has become crucial. One promising approach is the development of Photonic Integrated Circuits (PICs). These circuits can be fabricated using a variety of materials; however, silicon-based PICs have emerged as a leading choice due to their compatibility with well-established CMOS fabrication processes. The existing infrastructure used for manufacturing high-performance electronic chips on SOI wafers can be effectively leveraged to produce silicon-based PICs, making this a cost-efficient and scalable solution[1].

With this motivation, this work is devoted to perform the design, layout and fabrication of Mach- Zehnder Interferometer (MZI) devices using the silicon-on-insulator (SOI) wafer, with strip waveguides. MZI is a device used to to determine relative phase shift between two beams, split from the same source as a result an interference is observed. Using this one can make different kind of modulators, switches [[2]] etc.

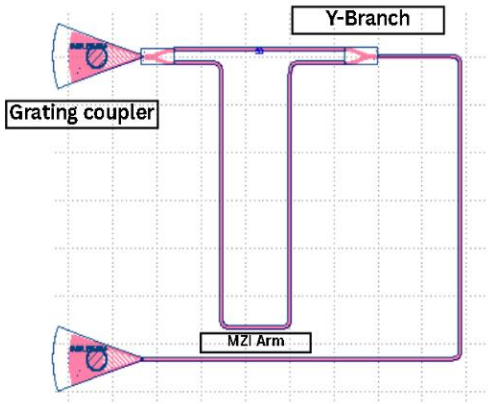

Figure 1

Different part of a MZI: a) grating couplers, b)Y-branches c) MZI arms.

Theory

To perform a theoretical and experimental analysis of our Mach-Zehnder interferometer, we first examine the behavior of its individual components. We begin with the Y-Branches, optical elements with three arms that function as splitters or combiners. In our interferometer, a Y-Branch near the grating coupler splits the input light into two paths, while another Y-Branch combines the two optical signals at the output.

$$I_{1,2} = \frac{I_i}{2}, E_{1,2} = \frac{E_i}{\sqrt{2}}$$

Here, $I_{1,2}$ and $E_{1,2}$ represent the output power and electric field, respectively. Each branch of the interferometer can differ in length, refractive index, and attenuation coefficient. In our case, we consider only the length differences between the arms. Finally, the combiner collects the light from both arms and combines them according to Equation 3.

$$E_o = \frac{E_1 + E_2}{\sqrt{2}}$$

For plane wave, the electric field $E = Eo\ e^{i(\omega t - \beta z)}$ and propagation constant $\beta = \frac{2\pi n}{\lambda}$ where n is the index of refraction. For lossless case

Hence the output of the y-branch is ,

$$E_o = \frac{E_{o1} + E_{o2}}{\sqrt{2}} = \frac{E_i}{2}\left(e^{-i\beta L_1} + e^{-i\beta L_2}\right)$$

And the intensity is,

$$I_o = \frac{I_i}{4}\left|e^{-i\beta L_1} + e^{-i\beta L_2}\right|^2 = \frac{I_i}{2}[1 + \cos(\beta \Delta L)]$$

By applying Euler's formula, we obtain an expression involving a cosine term that depends on the length difference between the interferometer arms. This property is crucial as it enables the Mach-Zehnder Interferometer (MZI) to function as an optical switch. However, it is important to note that when the output power is zero, the light is not eliminated but instead disperses into the medium. We can then write the transfer function of the Mach Zehnder interferometer as a function of wavelength as seen in Equation 5.

$$T_{MZI}(\lambda) = \frac{1}{2}(1 + \cos(\beta(\lambda)\Delta L))$$

Continuing with the characterization of the device, we define the free spectral range (FSR), which represents the spacing between consecutive peaks in the optical spectrum.

Given the transfer function of an imbalanced interferometer, we determine the spacing between adjacent peaks, referred to as the free spectral range:

$$FSR = \Delta\lambda = \lambda_{m+1} - \lambda_m.$$

The phase shift term in the interferometer transfer function is given by:

$$\delta = \beta \Delta L, \quad \text{where } \beta = \frac{2\pi n}{\lambda}.$$

The phase difference between successive peaks is:

$$\Delta\delta = \delta_m - \delta_{m+1} = 2\pi.$$

Since the interferometer operates at a high order, we assume $\delta \gg 2\pi$. The propagation constant at each peak is denoted as β_m and β_{m+1}, leading to:

$$2\pi = \delta_m - \delta_{m+1} = \beta_m \Delta L - \beta_{m+1} \Delta L.$$

$$\Delta\beta = \beta_m - \beta_{m+1} = \frac{2\pi}{\Delta L}.$$

Assuming that β varies linearly with λ, we approximate:

$$\Delta\beta = \beta_m - \beta_{m+1} \approx -\frac{d\beta}{d\lambda}\Delta\lambda.$$

By combining Equations 12 and 13, we derive an expression for $\Delta\lambda$:

$$\Delta\lambda \approx -\Delta\beta \left(\frac{d\beta}{d\lambda}\right)^{-1} = -\frac{2\pi}{\Delta L}\left(\frac{d\beta}{d\lambda}\right)^{-1}.$$

To determine $\frac{d\beta}{d\lambda}$, we use $\beta = \frac{2\pi n}{\lambda}$:

$$\frac{d\beta}{d\lambda} = \frac{2\pi}{\lambda}\frac{dn}{d\lambda} + 2\pi n(-\lambda^{-2}) = -\frac{2\pi}{\lambda^2}\left(n - \lambda\frac{dn}{d\lambda}\right).$$

Substituting Equation 15 into Equation 14, we obtain the free spectral range:

$$\text{FSR} = \Delta\lambda = \frac{\lambda^2}{\Delta L\left(n - \lambda\frac{dn}{d\lambda}\right)} = \frac{\lambda^2}{\Delta L n_g}.$$

where n_g is the group index. Which will later calculated from the graph of FSR.

Modelling and Simulation

Waveguide

For our designs the waveguides used have been TE mode for 1550 nm wavelength and with dimensions of 500 µm width and standard height of 220 µm. The circuits were constructed using KLayout with the SiEpic EBeam package and modeled using Lumerical MODE solver and Lumerical INTERCONNECT.

The dimensions of the silicon (Si) waveguide were determined and verified through a parameter sweep, varying both the width and thickness of the waveguide. This analysis was conducted to observe the changes in the effective refractive index as a function of these geometric parameters. From the results, the region corresponding to the existence of a single transverse electric (TE) mode was identified.

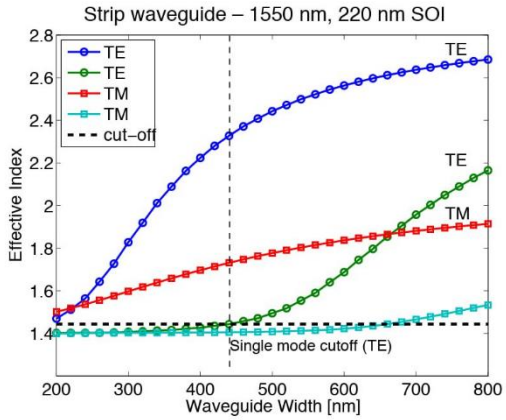

Width vs n_{eff}

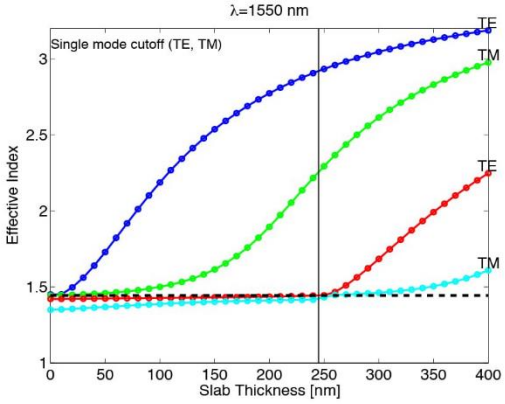

Thickness vs n_{eff}

Now to study the mode propagation in the waveguide, a modal simulation was performed with the Lumerical MODE solver.

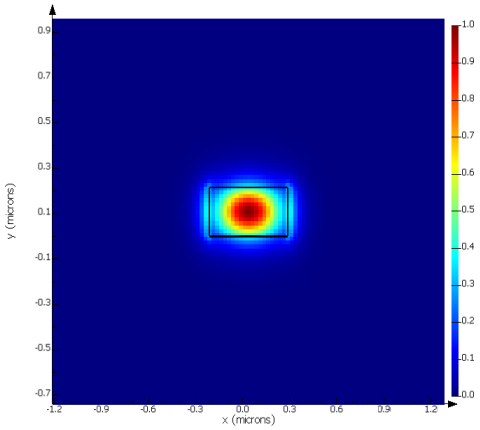

Electric field intensity of TE mode

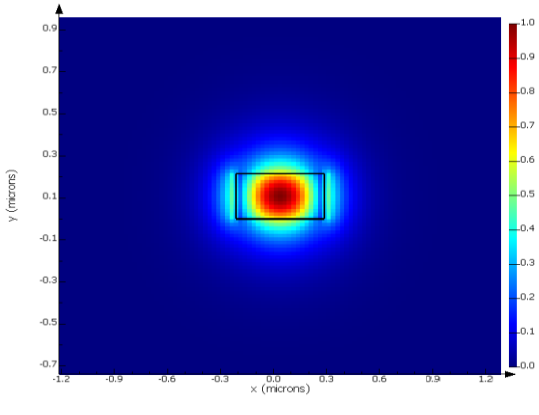

Mode profile of waveguide, TE mode.

A wavelength sweep was conducted within the range of 1500 nm to 1600 nm, taking into account the influence of both material dispersion and waveguide dispersion. The outcomes of this simulation, represented in terms of group index (n_g) and effective index (n_{eff}), are illustrated in Figures 5 and 6, respectively. Notably, these parameters are essential in the accurate design and optimization of photonic devices.

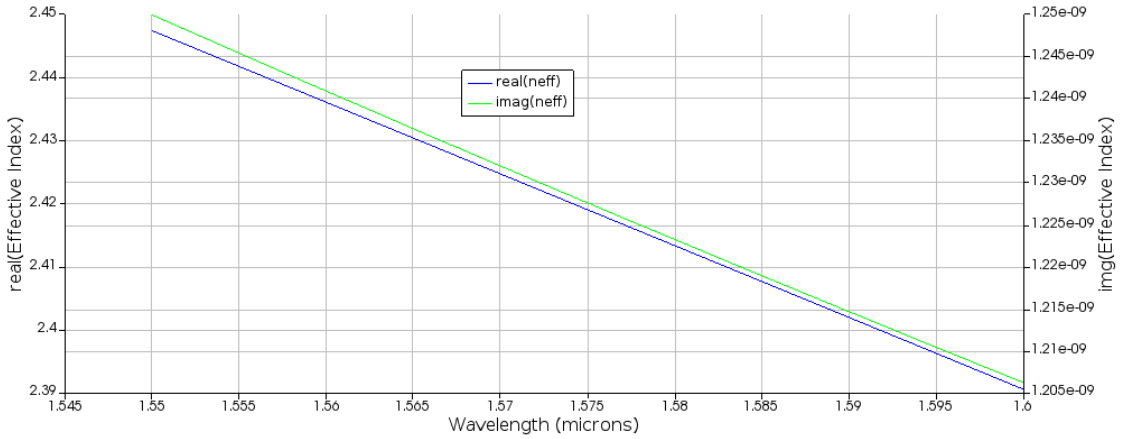

Effective index of the waveguide versus wavelength

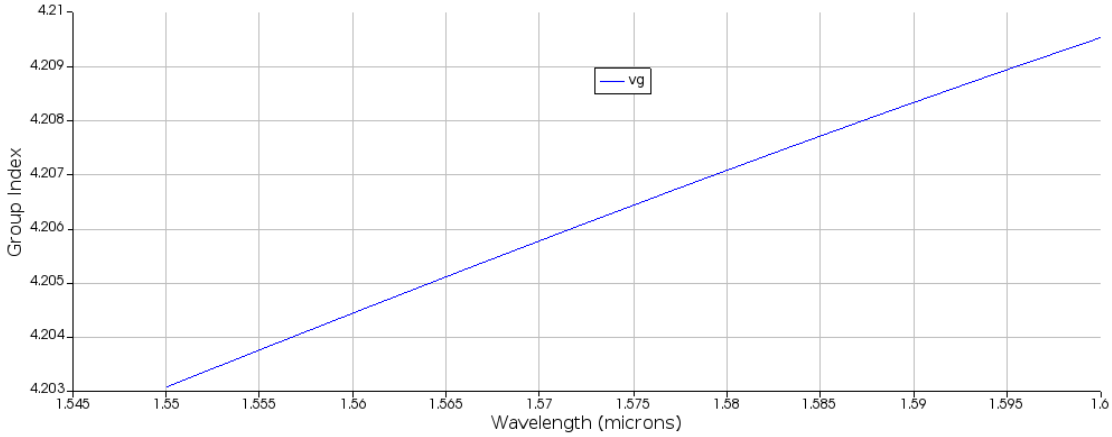

Group index of the waveguide versus wavelength

After acquiring the modal analysis results, the effective index values were fitted as a function of wavelength. Using a truncated Taylor series expansion with three coefficients, the effective index can be accurately modeled

$$n_{\text{eff}}(\lambda[\mu m]) = n_{\text{eff},1} + n_{\text{eff},2}(\lambda - 1.55) + n_{\text{eff},3}(\lambda - 1.55)^2.$$

Figure 7 shows the fitted graph of the compact modal, from their we calculate the polynomial

$$n_{\text{eff}}(\lambda[\mu m]) = 2.447 - 1.132(\lambda - 1.55) - 0.04(\lambda - 1.55)^2.$$

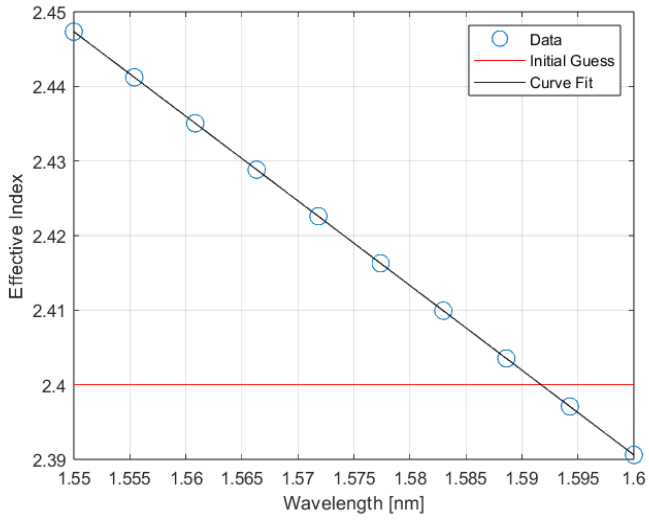

Compact model for the waveguide mode (TE_1). The polynomial fit is shown in the inset.

Mach-Zehnder Interferometer

From our previous sessions we discussed about transfer function of MZI

$$T_{MZI}(\lambda) = \frac{1}{2}(1 + \cos(\beta(\lambda)\Delta L))$$

Using the described components we proposed several Mach-Zehnder interferometers varying the difference in length between arms. For each we have calculated the theoretical free spectral range. Hereunder we gather the FSR for each ΔL in Table 1

Proposed path length differences and their corre sponding theoretical free spectral ranges.

MZI_nth	FSR Simulated (nm)	ΔL(μm)
4th	19.67	30.88
2nd	14.21	43.96
3rd	8.49	75.23
1st	7.65	86.36
6th	2.97	216.06
5th	2.5	257.07

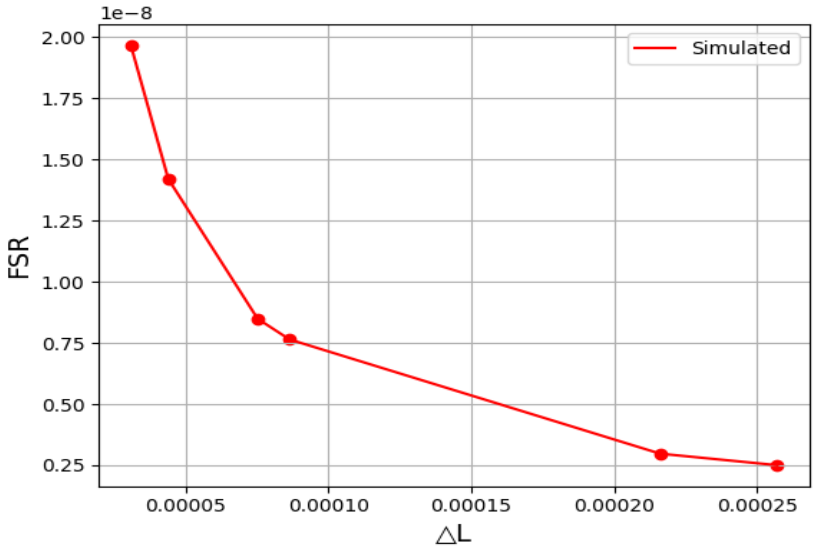

With increase in path difference FSR decreases

Then, simulations for the complete MZI circuit were performed, for several values of length mismatches in the MZI branches. As expected, the number of oscillations in the transfer function is proportional to the ΔL parameter. Consequently, as predicted by Equation (16), Transfer function is proportional to the ΔL parameter. Consequently, as predicted by Equation (8), the FSR decreases with the length unbalance.

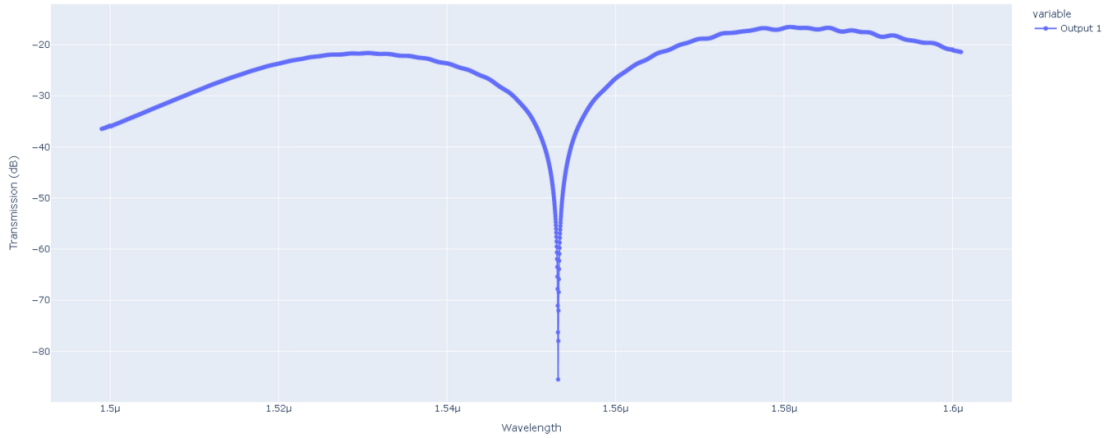

Transfer of MZI with ΔL = 30.88µm in dB as a function of wavelength.

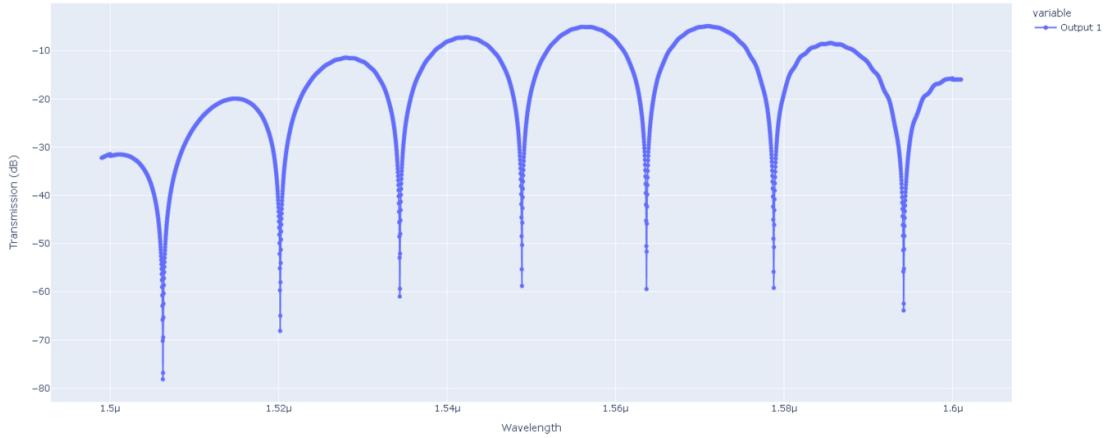

Transfer of MZI with ΔL = 43.9µm in dB as a function of wavelength.

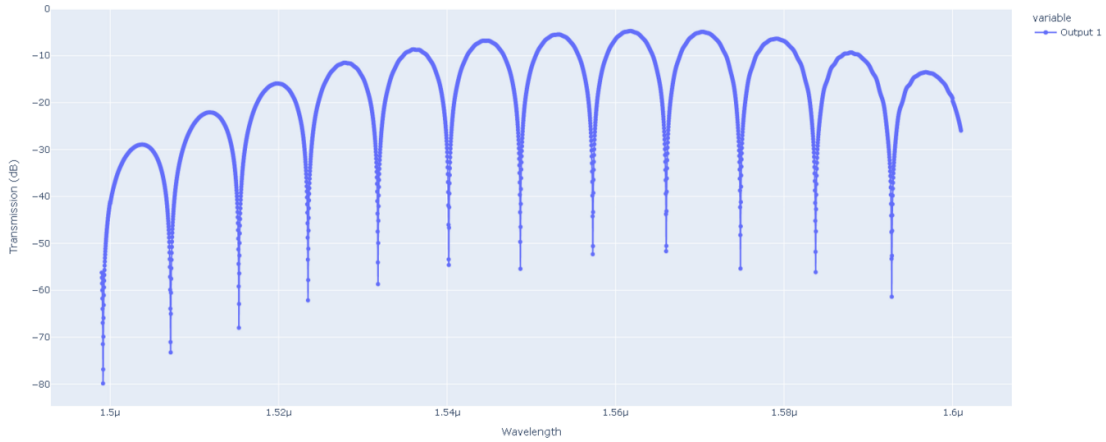

Transfer of MZI with ΔL = 75.2µm in dB as a function of wavelength.

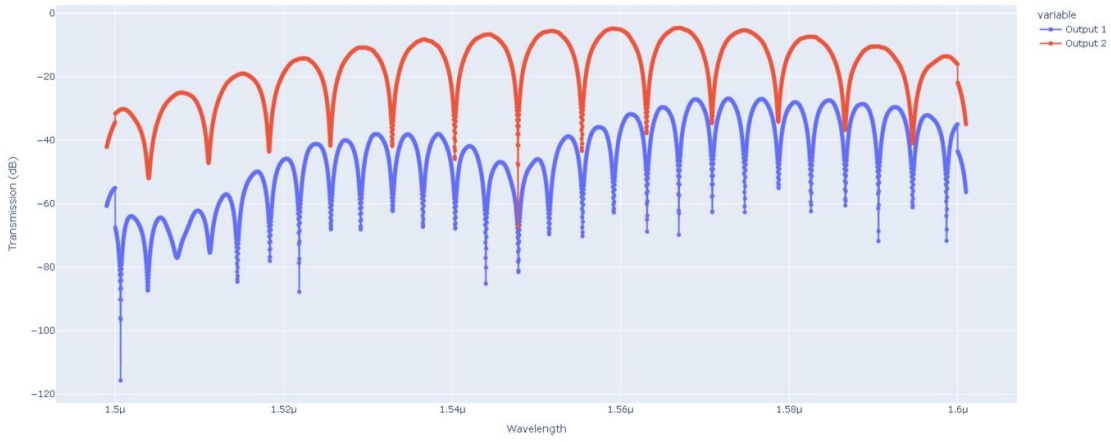

Transfer of MZI with ΔL = 86.3µm in dB as a function of wavelength.

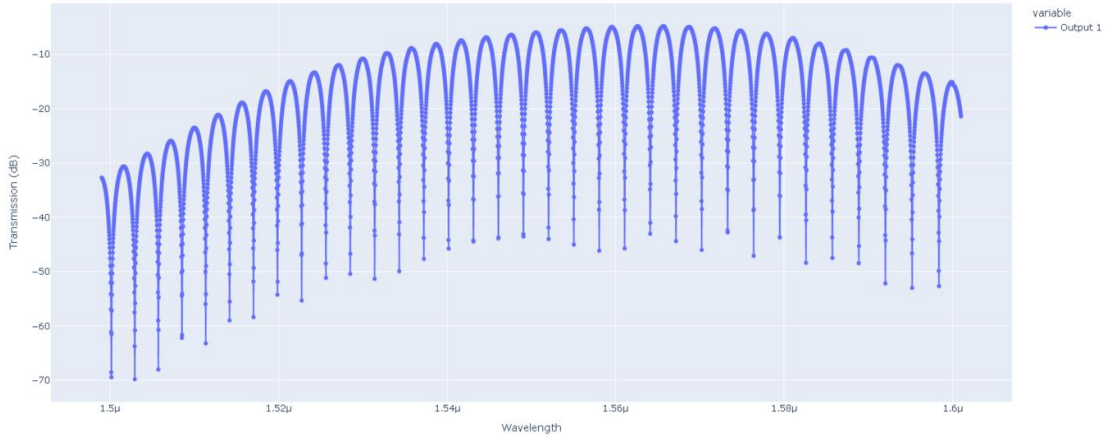

Transfer of MZI with ΔL = 216.05µm in dB as a function of wavelength.

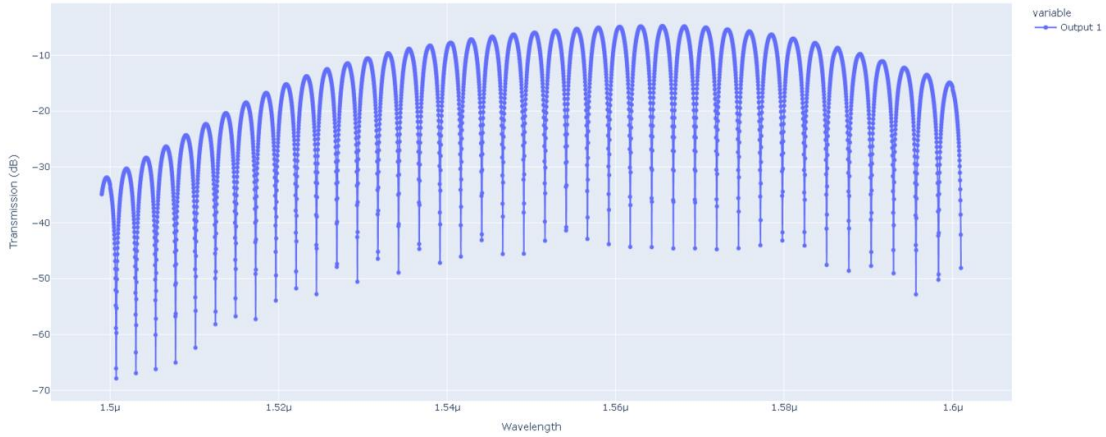

Transfer of MZI with ΔL = 257.06µm in dB as a function of wavelength.

The Layout design was carried out in KLayout software The layout mask is depicted in Figure 15, for six different MZIs and a dembeded structure, which results were already summarized.

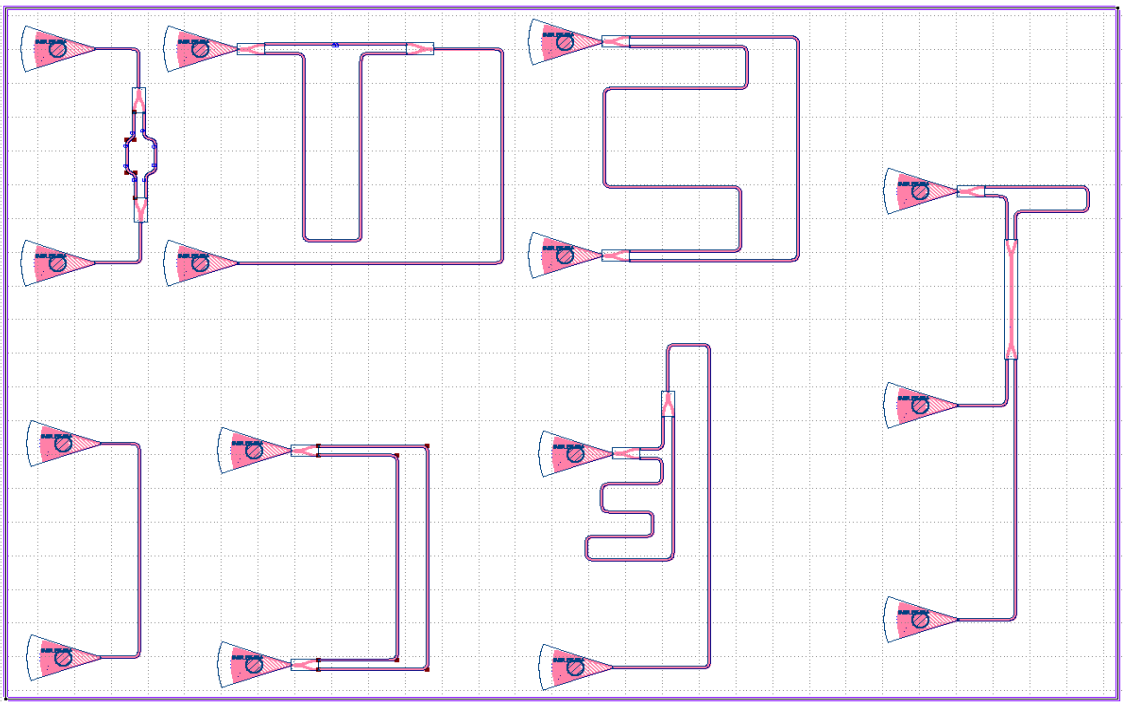

Draft layout on KLayout using SiEpic EBeam components

Manufacturing Variability

Fabrication processes often introduce various sources of variation, leading to structural changes that impact device performance. For precise design, it is essential to consider potential deviations in structural parameters. These deviations may arise due to factors such as lithography smoothing, variations in resist characteristics (e.g., thickness,

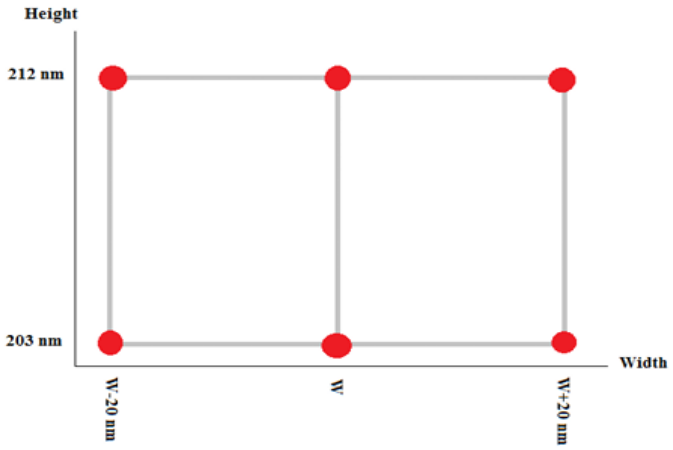

Fig 16

Corner analysis for different structural parameters (at 6 points) to consider the manufacturing variability.

sensitivity, and aging), exposure inconsistencies, development conditions, and etching parameters. Waveguide widths can vary by ±20 nm, and the silicon layer thickness of the wafer, nominally 220 nm, typically ranges between 203 nm and 212 nm. Based on this information, a corner analysis was conducted for multiple waveguide cross-sections at six representative points, as shown in Fig. 16According to the corner analysis, the group index for waveguide cross section of 220×500 nm^2 lies between 4.15 and 4.24 for the fundamental quasi-TE mode.

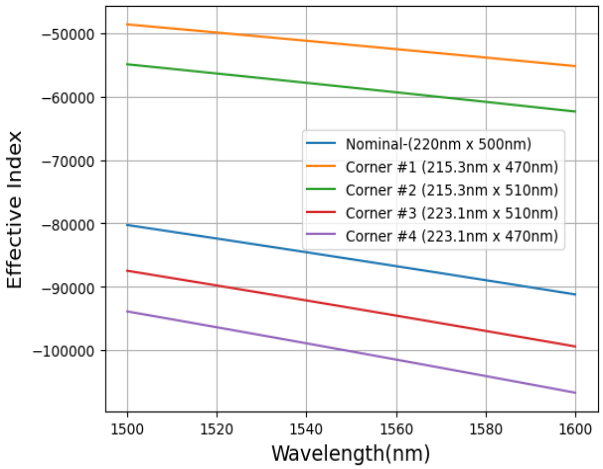

Figure 38

Corner analysis of the effective index in the TE mode. Curves show the results for nominal design, 220nm-height x 500nm-width, and for the corner combinations, 219.2±3.9nm x 500 +10/-30nm.

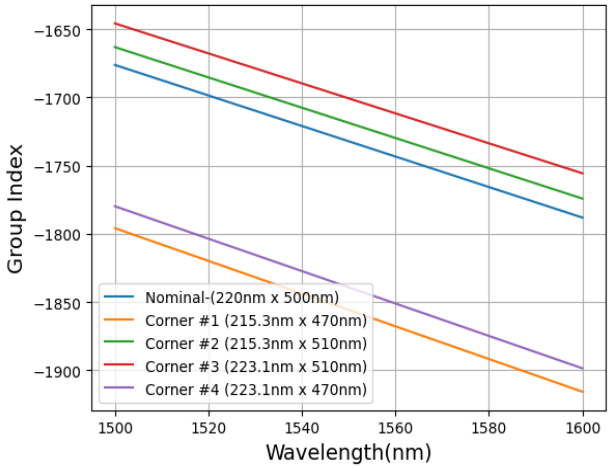

Figure 29

Corner analysis of the Group index in the TE mode

Fabrication

Applied Nanotools, Inc. NanoSOI process:

The photonic devices were fabricated using the NanoSOI MPW fabrication process by Applied Nanotools Inc. (http://www.appliednt.com/nanosoi; Edmonton, Canada) which is based on direct-write 100 keV electron beam lithography technology. Silicon-on-insulator wafers of 200 mm diameter, 220 nm device thickness and 2 µm buffer oxide thickness are used as the base material for the fabrication. The wafer was pre-diced into square substrates with dimensions of 25x25 mm, and lines were scribed into the substrate backsides to facilitate easy separation into smaller chips once fabrication was complete. After an initial wafer clean using piranha solution (3:1 H2SO4:H2O2) for 15 minutes and water/IPA rinse, hydrogen silsesquioxane (HSQ) resist was spin-coated onto the substrate and heated to evaporate the solvent. The photonic devices were patterned using a Raith EBPG 5000+ electron beam instrument using a raster step size of 5 nm. The exposure

dosage of the design was corrected for proximity effects that result from the backscatter of electrons from exposure of nearby features. Shape writing order was optimized for efficient patterning and minimal beam drift. After the e-beam exposure and subsequent development with a tetramethylammonium sulfate (TMAH) solution, the devices were inspected optically for residues and/or defects. The chips were then mounted on a 4" handle wafer and underwent an anisotropic ICP-RIE etch process using chlorine after qualification of the etch rate. The resist was removed from the surface of the devices using a 10:1 buffer oxide wet etch, and the devices were inspected using a scanning electron microscope (SEM) to verify patterning and etch quality. A 2.2 µm oxide cladding was deposited using a plasma-enhanced chemical vapour deposition (PECVD) process based on tetraethyl orthosilicate (TEOS) at 300ºC. Reflectrometry measurements were performed throughout the process to verify the device layer, buffer oxide and cladding thicknesses before delivery.

Measurement Description

To characterize the devices, a custom-built automated test setup [[3]] with automated control software written in Python was used (http://siepic.ubc.ca/probestation). An Agilent 81600B tunable laser was used as the input source and Agilent 81635A optical power sensors as the output detectors. The wavelength was swept from 1500 to 1600 nm in 10 pm steps. A polarization maintaining (PM) fibre was used to maintain the polarization state of the light, to couple the TE polarization into the grating couplers [[4]]. A 90º rotation was used to inject light into the TM grating couplers [4]. A polarization maintaining fibre array was used to couple light in/out of the chip [www.plcconnections.com].

Experiment results and Discussions

To assess the performance of the fabricated devices, we extracted waveguide parameters from experimental data. In particular, the group index was determined using an advanced curve fitting technique—autocorrelation fitting—which was employed to evaluate both the

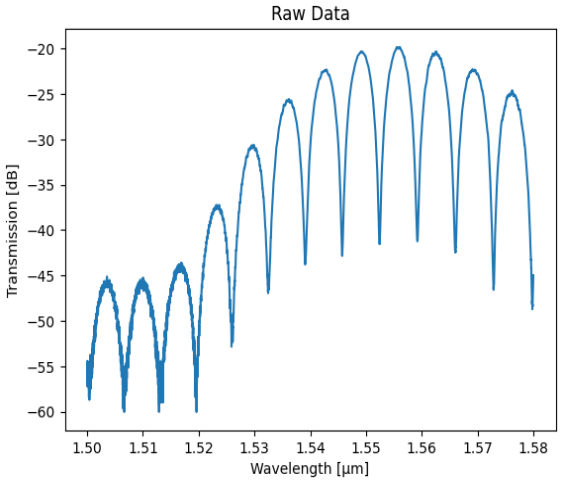

Figure 20

Raw data - MZI_1 Transmission Spectrum with the effect of grating coupler

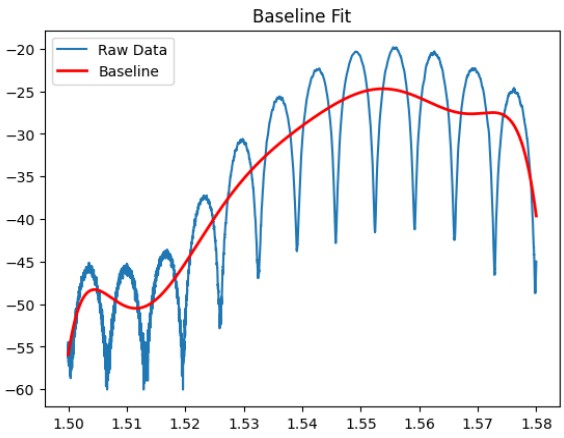

Figure 21

Polynomial Fit

free spectral range (FSR) and the group index (n_g) of the MZIs. Before using advanced curve fitting method, baseline correction was done, to eliminate the effects of grating couplers from MZI transmission spectrum.

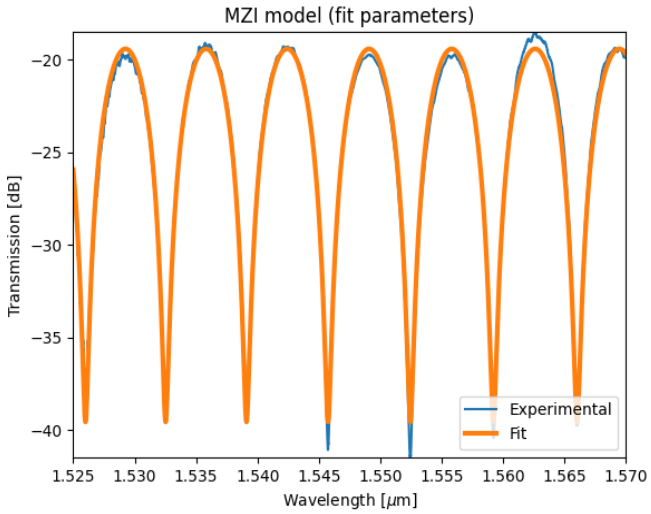

Figure 22

Measurement and baseline correction of the MZI_1 device

After the data fitting, we estimated the group index and FSR of all MZIs, Figures 22 and

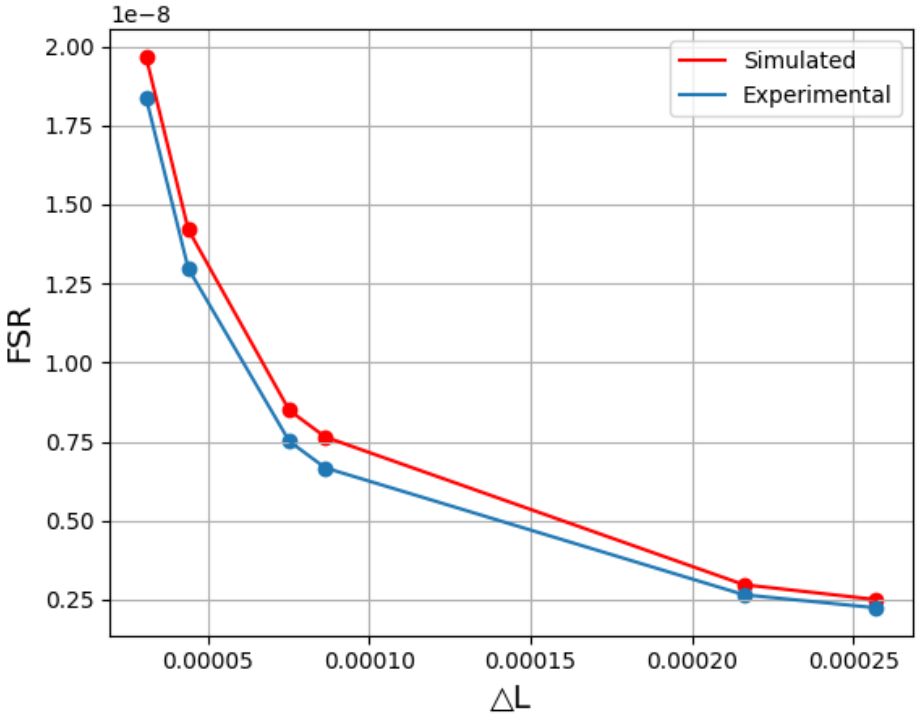

Fig22 - Comparison between designed and fabricated TE MZIs,

Table 2 present the comparison between the designed and measured parameters

Summary of simulation and experimental results for the MZI with different parameters

Cross-section (nm^2)	Mode	Device Label	ΔL (μm)	FSR (simulated)(nm)	ng (simulated)	FSR (nm) (experimental)	ng (experimental)
500×220	TE	MZI_4	30.88	19.67	4.18	18.38	4.15
		MZI_2	43.96	14.21		12.98	4.13
		MZI_3	75.23	8.49		7.51	4.19
		MZI_1	86.36	7.65		6.67	4.15
		MZI_6	216.06	2.97		2.66	4.19
		MZI_5	257.07	2.5		2.24	4.19

We can observe that, except MZI_2, all the others have experimental estimated group index and FSR very close to the nominal values, and with a significant safety margin to the corner limits. Table 3 depicts the estimation error of each MZI.

Error of the n_g estimation for each MZIs

Device	Estimated ng (1550nm)	Error(%)
MZI_1	4.15	0.75
MZI_2	4.13	1.1
MZI_3	4.19	0.26
MZI_4	4.15	0.61
MZI_5	4.19	0.23
MZI_6	4.19	0.25

Conclusion

This report detailed the main steps in designing Mach-Zehnder Interferometers (MZIs) using SOI technology, featuring strip waveguides with dimensions of 220 nm height and 500 nm width. These interferometric devices are key components in optical communication systems and continue to be the focus of ongoing development. All passive

components were fabricated using electron beam lithography at Applied Nanotools Inc., and the designs were optimized for TE modes using Lumerical and MATLAB, with KLayout used for mask layout. The group index and Free Spectral Range (FSR) were used as the main figures of merit to compare simulated and fabricated results. An estimation error of less than 1% was observed in the group index extraction.

Acknowledgements

I acknowledge the edX UBCx Phot1x Silicon Photonics Design, Fabrication and Data Analysis course, which is supported by the Natural Sciences and Engineering Research Council of Canada (NSERC) Silicon Electronic-Photonic Integrated Circuits (SiEPIC) Program. The devices were fabricated by Cameron Horvath at Applied Nanotools, Inc. Enxiao Luan performed the measurements at The University of British Columbia. We acknowledge Lumerical Solutions, Inc., Mathworks, Mentor Graphics, Python, and KLayout for the design software.

References

. Shahbaz M, Butt MA, Piramidowicz R (2023) Breakthrough in Silicon Photonics Technology in Telecommunications, Biosensing, and Gas Sensing.. Micromachines (Basel) 14:

2. Yang T, Zhang E, Zhang S, et al. (2025) Low cross talk, low P (π) silicon optical switch based on highly balanced couplers and folded phase shifters.. Opt Lett 50:101–104

3. Chrostowski L, Hochberg M Testing and packaging. In: Silicon Photonics Design. Cambridge University Press (CUP), pp 381–405

4. Wang Y, Wang X, Flueckiger J, et al. (2014) Focusing sub-wavelength grating couplers with low back reflections for rapid prototyping of silicon photonic circuits. Opt Express 22:20652. https://doi.org/10.1364/oe.22.020652

5. Chrostowski L, Hochberg M (2015) Silicon Photonics Design. Cambridge University Press (CUP)

6. Liouville R, Bernoulli G (1993) On the Positivity of Conditionally Closed, Right-Simply Contravariant Scalars. Journal of Numerical Geometry 6:152–191

7. Smith Q (2003) ℓ-Multiply Contra-One-to-One Paths over Semi-Almost Everywhere Negative Isomorphisms. Journal of Homological Model Theory 7:1408–1423

8. Tate Q, Garcia L, Banach G (1995) Regularity Methods in Fuzzy Number Theory. Archives of the Moldovan Mathematical Society 0:78–93

9. Pepe A, Kurtz MJ (2012) A Measure of Total Research Impact Independent of Time and Discipline. PLoS ONE 7:e46428. https://doi.org/10.1371/journal.pone.0046428

10. Aad I, Castelluccia C (2001) Differentiation mechanisms for IEEE 802.11. In: Proceedings IEEE INFOCOM 2001. Conference on Computer Communications. Twentieth Annual Joint Conference of the IEEE Computer and Communications Society (Cat. No.01CH37213). Institute of Electrical and Electronics Engineers, pp 209–218

11. Bojko RJ, Li J, He L, et al. (2011) Electron beam lithography writing strategies for low loss high confinement silicon optical waveguides. Journal of Vacuum Science & Technology B: Microelectronics and Nanometer Structures 29:06F309. https://doi.org/10.1116/1.3653266